

Three-dimensional active turbulence in microswimmer suspensions: simulations and modelling.

A. Gascó,¹ I. Pagonabarraga,^{1,2} and A. Scagliarini^{3,4,*}

¹*Departament de Física de la Matèria Condensada, Universitat de Barcelona,
Carrer de Martí i Franquès, 08028 Barcelona, Spain*

²*Universitat de Barcelona Institute of Complex Systems (UBICS),
Universitat de Barcelona, 08028 Barcelona, Spain*

³*Istituto per le Applicazioni del Calcolo (IAC), Consiglio Nazionale
delle Ricerche (CNR), Via dei Taurini 19, 00185 Rome, Italy*

⁴*INFN, sezione Roma “Tor Vergata”, via della Ricerca Scientifica 1, 00133 Rome, Italy*

Active turbulence is a paradigmatic and fascinating example of self-organized motion at large scales occurring in active matter. We employ massive hydrodynamic simulations of suspensions of resolved model microswimmers to tackle the phenomenon in semi-dilute conditions at a mesoscopic level. We measure the kinetic energy spectrum and we detect a k^{-3} power law regime. The velocity distributions are of Lévy type, a distinct difference with inertial turbulence. Furthermore, we propose a reduced order dynamical deterministic model for active turbulence, inspired to *shell models* for classical turbulence, whose numerical and analytical study confirms the spectrum power-law observed in the simulations and reveals hints of a non-Gaussian, intermittent, physics of active turbulence. Direct numerical simulations and modelling also agree in pointing to a phenomenological picture whereby, in the absence of an energy cascade *à la Richardson* forbidden by the low Reynolds number regime, it is the coupling between fluid velocity gradients and bacterial orientation that gives rise to a multiscale dynamics.

I. INTRODUCTION

One of the most striking features of active systems is the emergence of correlated motion and structures on scales much larger than that of the single agents. Forms of self-organized motion are ubiquitous in Nature [1], from colonies of microorganisms [2–4] to flocks of birds and fish schools [5, 6]. Collective motion in microbial suspensions, in particular, appears as a tangle of coherent structures, like vortices, jets, that recall those typically encountered in turbulent flows. This morphological analogy suggested to introduce the term *bacterial* or *active turbulence* [7–10]. But *what is turbulence*? Borrowing a celebrated quote, it is “hard to define, but easy to recognize when we see it!” [11]. Is, then, visual inspection enough? Certainly not, as witnessed by the consistent body of works devoted to a quantitative description of complex motion in active systems and of its relation with turbulence. Power-law decays of kinetic energy spectra over unexpectedly wide ranges of wavenumbers have been identified as a signature of turbulent behaviour in diverse systems including dense bacterial suspensions [12, 13], collections of ferromagnetic spinners [14], active nematics [15, 16], synthetic swimmers at interfaces [17], among others. Nevertheless, a *universality* of some kind seems to be lacking [13, 18], unlike in classical turbulence, where Kolmogorov’s theory of the inertial range constitutes a key, unifying ingredient [19]. With the aim of analyzing multiscale interactions and energy transfer, recent studies have focused on the spectral properties of continuum models [20–25], where the active fluid is described as an effective medium, whose equations are inspired by nematodynamics [26–29] and pattern formation [13, 30]. In all such approaches, it is surmised that the modelled system, be it a bacterial suspension or an active gel, is highly concentrated, such that the interactions among active agents are essentially excluded volume and alignment. On the other hand, in the limit of extreme dilution (i.e. for volume fractions below the onset of collective motion), it has been shown theoretically that, due to long-range hydrodynamic interactions, suspensions of extensile microswimmers (“pushers”) develop a solvent velocity field with variance anomalously growing with the volume fraction and kinetic energy spectra whose functional form can be derived analytically with a kinetic theory approach [31–33]. In semi-dilute conditions, hydrodynamically induced correlations engender collective motion and large-scale flows [34–37]. In this context, power-law spectra have been measured in numerical simulations of suspensions of point-like and slender rod-like microswimmers [32, 37]. However, despite these few relevant exceptions, the phenomenon of active turbulence in semi-dilute situations, namely far from close packing but above the onset of collective motion, has been much less investigated and is still poorly understood from a theoretical point of view. So, the goal of the present paper is twofold. On one hand, we will describe active turbulence signatures in semi-dilute suspensions of model

* andrea.scagliarini@cnr.it

spherical swimmers (squirmers); on the other we will propose a novel theoretical framework helping to understand the mechanisms underlying active turbulence phenomenology.

To this aim, we perform large scale direct numerical simulations (DNS) of suspensions of pushers, where the solvent hydrodynamics is fully resolved, both from the near to the far field. We characterize the solvent velocity field in terms of its energy spectra and probability density functions (PDFs). The spectrum displays a *plateau* at small wavenumbers, consistently with theoretical predictions [32, 33] for very dilute systems, followed by an algebraic decay, k^{-3} , signalling the presence of fluid motion on scales up to roughly half a decade larger than the microswimmer's size. We also introduce a reduced order dynamical deterministic model of active turbulence, pertaining to the class of the so called *shell models*, motivated by their successful story as turbulence models [38]. Having at disposal a shell model of active turbulence allows to study the statistical properties and chaotic behaviour of a computationally and theoretically challenging phenomenon within a low number of degrees-of-freedom description, which is, to some extent, even amenable of analytical treatment, as we also prove. The analysis of the shell model reproduces the kinetic energy spectrum power-law observed in the DNS. The shape of the velocity variables PDFs break scale-invariance, a hallmark of intermittency. The shell model leverages a phenomenological picture, confirmed by the DNS, whereby the coupling between the fluid velocity gradients and the bacterial orientation dynamics is the mechanism responsible for the generation of flow at large scales.

II. METHODS

The solvent hydrodynamics is simulated using a standard $D3Q19$ lattice Boltzmann method [39–41]. The microswimmers are modelled as solid spheres of radius R , mass $M = \frac{4}{3}\pi R^3 \rho_p$ (where ρ_p is the microswimmer density) and moment of inertia $I = \frac{2}{5}MR^2$. The momentum/torque exchange in fluid-solid coupling is ensured by the so called bounce-back-on-links algorithm [42–44]. The swimming mechanism is introduced via a minimal implementation of the “squirmers” model [45, 46], whereby a non-zero tangential polar component of the axisymmetric slip velocity profile, depending on the two parameters B_1 and B_2 , is imposed at the particle surface

$$\mathbf{u}_s = (B_1 \sin \theta + B_2 \sin \theta \cos \theta) \hat{\theta}, \quad (1)$$

where $\theta = \arccos(\hat{\mathbf{e}} \cdot \hat{\mathbf{r}}_s)$ is the angle between the squirmer orientation unit vector, $\hat{\mathbf{e}}$, and the position on the particle surface, $\hat{\mathbf{r}}_s = \frac{\mathbf{x}_s - \mathbf{X}}{R}$, relative to the position of its centre of mass, \mathbf{X} (i.e. it is the polar angle for a spherical coordinate system in a frame comoving with the particle and $\hat{\theta}$ is its associated unit vector). With the prescription (1) for the surface slip, the squirmer generates a velocity field at the position \mathbf{x} that, to leading orders, takes the form

$$\mathbf{U}(\mathbf{x}, t) = B_1 \left(\left(\frac{R}{r} \right)^3 (\hat{\mathbf{e}} \cdot \hat{\mathbf{r}}) \hat{\mathbf{r}} - \frac{1}{3} \left(\frac{R}{r} \right)^3 \hat{\mathbf{e}} - \frac{1}{2} \beta \left(\frac{R}{r} \right)^2 (3(\hat{\mathbf{e}} \cdot \hat{\mathbf{r}})^2 - 1) \hat{\mathbf{r}} \right) + O \left(\left(\frac{R}{r} \right)^4 \right) \quad (2)$$

where $\mathbf{r} = \mathbf{x} - \mathbf{X}(t)$, $r = |\mathbf{r}|$, $\hat{\mathbf{r}} = \frac{\mathbf{r}}{r}$ and $\beta \equiv B_2/B_1$ ($\beta < 0$ since we are considering here pushers) determines the amplitude of the stress exerted by the microswimmer on the surrounding fluid. The equations of motion for the centre of mass position $\mathbf{X}^{(i)}(t)$, barycentric velocity $\mathbf{V}^{(i)}(t)$, intrinsic orientation $\hat{\mathbf{e}}^{(i)}(t)$ and angular velocity $\boldsymbol{\Omega}^{(i)}(t)$ of the i -th squirmer ($i = 1, 2, \dots, N$) read:

$$\begin{aligned} \dot{\mathbf{X}}^{(i)} &= \mathbf{V}^{(i)} \\ \dot{\mathbf{V}}^{(i)} &= \frac{1}{M} (\mathbf{F}_h + \mathbf{F}_a - \chi \mathbf{V}^{(i)}) \\ \dot{\hat{\mathbf{e}}}^{(i)} &= \boldsymbol{\Omega}^{(i)} \wedge \hat{\mathbf{e}}^{(i)} \\ \dot{\boldsymbol{\Omega}}^{(i)} &= \frac{1}{I} (\mathbf{T}_h - \zeta \boldsymbol{\Omega}^{(i)}), \end{aligned} \quad (3)$$

where $\mathbf{F}_a \propto \int_{\mathcal{S}} \mathbf{u}_s d\mathbf{x}_s$ is the force determining the self-propulsion (an equal in magnitude and opposite sign is imparted to the fluid such that, globally, the system is force-free), \mathbf{F}_h and \mathbf{T}_h are force and torque arising from the flows generated in the solvent (and responsible, therefore, for hydrodynamic interactions among particles) and χ and ζ are friction coefficients. Equations (3) are solved numerically, time-marching first the positions and orientations vector by means of a forward-Euler scheme, and then the velocities and angular velocities by means of an implicit (backward-Euler) update. The over-damped limit of (3) yields $\mathbf{V}^{(i)} \propto \Gamma^{-1}(\mathbf{F}_h + \mathbf{F}_a)$; in particular, for an isolated squirmer, this endows the particle with a self-propulsion velocity $V_p = \frac{2}{3}B_1\hat{\mathbf{e}}$. The method has been extensively tested and applied to various physical problems, including, among others, pairwise hydrodynamic interactions, the formation

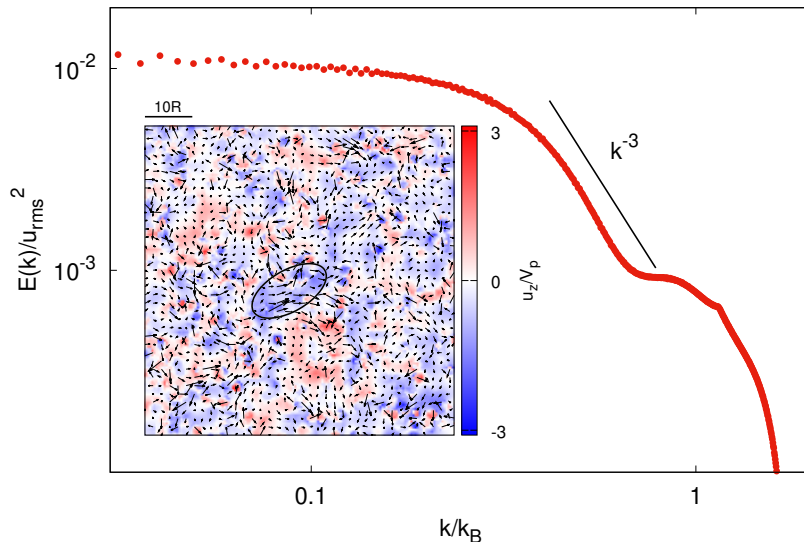


FIG. 1. MAIN PANEL: Energy spectrum (time-averaged over the statistically stationary state) of the fluid velocity field, normalized by the mean square velocity u_{rms}^2 , in a suspension of pushers ($\beta = -5$) at a volume fraction $\phi \approx 0.1$ (wavenumbers are normalized by $k_B = 2\pi/R$); the solid line indicates the scaling $E(k) \sim k^{-3}$. INSET: Snapshot of the velocity field in the plane $z = L/2$ from a simulation: the in-plane vectors (u_x, u_y) are depicted as arrows and the out-of-plane component u_z (rescaled by the characteristic swimming speed V_p) as a color map. Notice the size of correlated regions as compared to the microswimmer size $\sim R$; in particular, the occurrence of a *jet* extending on a scale of several particle radii is highlighted by the black ellipse.

of polar order, clustering and sedimentation in suspensions of microswimmers [47–50].

We perform numerical simulations in a triperiodic cubic box of side $L = 512$ lattice points, with $N \approx 2.6 \times 10^5$ pushers of radius $R = 2.3$ lattice units (corresponding to a volume fraction of $\phi \approx 0.1$) and $\beta = -5$ (for this value of β the system does not develop a global polar order [48, 51]). The first squirming parameter is set to $B_1 = 1.5 \times 10^{-3}$, so the intrinsic self-propulsion speed is $V_p = 10^{-3}$, in lattice Boltzmann units (lbu). The kinematic viscosity is $\nu = 1/6$ lbu such that the Reynolds number at the particle scale, for an isolated microswimmer, is $\text{Re}_p \approx 10^{-2}$.

III. RESULTS

A. Numerical simulations

In Fig. 1 we report the energy spectrum $E(k) = \frac{1}{2} \overline{\langle \tilde{\mathbf{u}}^* \cdot \tilde{\mathbf{u}} \rangle}$, where $\tilde{\mathbf{u}}(\mathbf{k})$ is the Fourier transform of the fluid velocity field and the overlined brackets, $\overline{\langle \cdot \rangle}$, indicate a surface integral on spheres of radius k , in spectral space, and time averaging over the statistically stationary state (wavenumbers are normalized by $k_B = 2\pi/R$). The spectrum shows a *plateau*, $E(k) \sim \text{const}$, at small wavenumbers, followed by an algebraic decay, $E(k) \sim k^{-3}$. This decay covers a relatively short range of wavenumbers. We must stress, though, that scaling ranges of limited extension (typically less than a decade) are a distinctive feature of a large variety of active systems [13, 16, 22, 52, 53]. A constant spectrum is the theoretical expectation for an ideal system of weakly interacting point-like stresslets [31–33], i.e. in the limit of extreme dilution. As the concentration increases, non-linearities stemming from hydrodynamic interactions among particles are expected to determine the development of a power-law profile of the spectrum, with a slope that depends on the volume fraction [32, 37, 52]. Remarkably, though, as shown in recent experiments with *E. Coli*, the exponent tends to approach the limiting value of ~ -3 as the systems enters the active turbulence regime [52]. It might be expected, despite the lack of a formal proof, that such an asymptotic behaviour holds only under semi-dilute conditions, i.e. below the close packing volume fraction, above which the physics of collective behaviour hinges on different mechanisms. Another peculiar aspect of the complex non-linear phenomenology of inertial turbulence is intermittency, which is intimately related to the breakup of global scale invariance [19]. Intermittency can be detected in 3D turbulent velocity fields looking at the probability density functions (PDFs) of longitudinal velocity

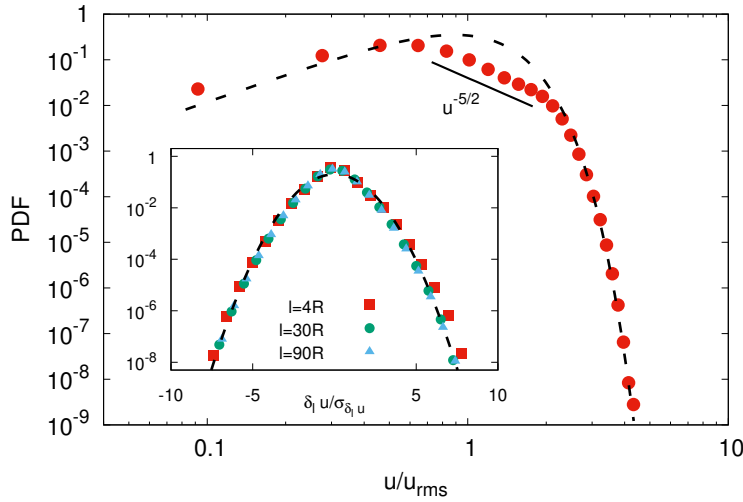


FIG. 2. MAIN PANEL. Probability density function of the fluid velocity magnitude (normalized by its root mean square value); the dashed line represents the χ -like distribution $\propto u^2 e^{-\frac{u^2}{2\sigma^2}}$ (with $\sigma \approx 0.63$), whereas the solid line highlights the algebraic decay $\propto u^{-5/2}$. INSET. Probability density functions of the longitudinal velocity increments, $\delta_l u = [\mathbf{u}(\mathbf{x} + \mathbf{l}, t) - \mathbf{u}(\mathbf{x}, t)] \cdot \frac{\mathbf{l}}{l}$ (divided by their standard deviation, $\sigma_{\delta_l u}$), for three separations $l/R = 4, 30, 90$. The dashed line depicts the Gaussian probability density function with zero mean and standard deviation $\sigma \approx 1.27$.

increments $\delta_l u = [\mathbf{u}(\mathbf{x} + \mathbf{l}, t) - \mathbf{u}(\mathbf{x}, t)] \cdot \frac{\mathbf{l}}{l}$. Upon proper rescaling, such to have a fixed variance, the PDFs do not attain a scale-independent functional form: they are Gaussian when the separation is of the order of the system size, $l \sim L$ (the so called “integral scale”), but become more and more *fat-tailed* at decreasing l (or, equivalently, the *flatness* grows as $l \rightarrow 0$). In contrast, in our simulations, as shown in Fig. 2 (inset), the PDFs seem to collapse onto a Gaussian curve for all l . As for the statistics of fluid velocity, we observe from the main panel of Fig. 2 that the PDF is well fitted by a χ -like distribution, i.e. it follows a Gaussian statistics, for small ($u \ll u_{\text{rms}}$) and large ($u \gg u_{\text{rms}}$) velocities, consistently with theoretical results obtained for suspensions of swimmers generating algebraically decaying flow fields, with a short range regularization [54]. At intermediate values the PDF is expected to deviate from Gaussianity; here, in particular, we find a good fit by a power law with the exponent $-5/2$, which is what would stem from a superposition of swimmers uniformly distributed in space, with associated velocity fields decaying as $U(r) \sim r^{-2}$ [55].

B. A reduced order deterministic model of active turbulence

One may wonder whether and to which extent it is possible to extend concepts and tools developed for inertial turbulence to active turbulence. To this end, we introduce a *shell model* for active turbulence that will generalize and rationalize the observed results. Shell models (SMs) are deterministic dynamical systems that reduce the complexity of the full (field) equations, though retaining some of their essential features. Originally introduced as a proxy of the Navier-Stokes equations, they represent a low number of degrees-of-freedom description of hydrodynamic turbulence. As such, they offer the possibility to investigate the chaotic dynamics and multiscale correlations of turbulence with obvious computational advantages [19, 38, 56–58]. Mathematically, SMs consist of a set of coupled ordinary differential equations, describing the time evolution of complex variables, $\tilde{u}_n(t)$ (with $n = 1, 2, \dots, N_s$), that can be thought of as Fourier amplitudes of velocity fluctuations over a length scale with associated wavenumber k_n . SMs do not carry any of the *geometrical* information contained in the original system, as \tilde{u}_n and k_n are both scalar variables. k_n stands for a radial coordinate in spectral space, whence the name *shell* (correspondingly, the discrete index n is called shell index). Recently, SMs have been extended to polymeric solutions, to address drag reduction and elastic turbulence [59–61][62]. Hydrodynamic theories describe active suspensions in terms of the bacteria concentration field, $c(\mathbf{x}, t)$, the (incompressible) fluid velocity field, $\mathbf{u}(\mathbf{x}, t)$, and an order parameter quantifying the degree of local orientation $\mathbf{p}(\mathbf{x}, t)$, which represents the average, within a fluid element, of the particle intrinsic swimming director, $p_i \propto \langle \hat{e}_i \rangle$. At odds with concentrated conditions, where the lack of alignment interactions rules out the local orientation \mathbf{p} as an appropriate field variable, in semi-dilute suspensions hydrodynamic interactions can induce locally (and, under

certain circumstances, even globally) polar order [48, 51, 63]. If we assume, for simplicity, that the microswimmers spatial distribution remains homogeneous in time ($c(\mathbf{x}, t) \approx c_0$, which is indeed confirmed by the DNS; consequently we also assume the field \mathbf{p} to be divergence-free), the equations of motion read [64–68],

$$\begin{aligned} \rho(\partial_t \mathbf{u} + \mathbf{u} \cdot \nabla) \mathbf{u} &= -\nabla P + \eta \nabla^2 \mathbf{u} + \nabla \cdot \sigma^{(a)} \\ \partial_t \mathbf{p} + (\mathbf{u} + w\mathbf{p}) \cdot \nabla \mathbf{p} &= \Omega \cdot \mathbf{p} - \Gamma \mathbf{p} + D \nabla^2 \mathbf{p}; \end{aligned} \quad (4)$$

$\sigma_{ij}^{(a)} = \zeta p_i p_j$ [65] is the active stress, where ζ is proportional to the swimmers' volume fraction and to the amplitude of the generated stresslet and, therefore, quantifies the level of activity. $\Omega_{ij} = \frac{1}{2}(\partial_i u_j - \partial_j u_i)$ denotes the antisymmetric part of the velocity gradient tensor, and η and D are the fluid dynamic viscosity and the orientation field diffusion coefficient, respectively. Except for the term $w(\mathbf{p} \cdot \nabla)\mathbf{p}$, Eqs. (4) closely resemble the Oldroyd-B equations for the polymer conformation [69], in vectorial form [59].

Inspired by this formal analogy, we can write a shell model for active fluids, with the inclusion of the self-propulsion, that will couple the dynamics of \tilde{u}_n with an equation for \tilde{p}_n , the amplitude of orientation magnitude fluctuations at the wavenumber k_n . To this aim, we first need to introduce the following operator [60] (we will omit hereafter the tilde (\dots) , for the sake of lightening the notation)

$$\begin{aligned} \Phi_n^{(\varepsilon)}(u, v) &= k_n [(1 - \varepsilon)u_{n+2}v_{n+1}^* + (2 + \varepsilon)u_{n+1}^*v_{n+2}] + \\ &= k_{n-1} [(2\varepsilon + 1)u_{n-1}^*v_{n+1} - (1 - \varepsilon)u_{n+1}v_{n-1}^*] + \\ &= k_{n-2} [(2 + \varepsilon)u_{n-1}v_{n-2} + (2\varepsilon + 1)u_{n-2}v_{n-1}] \end{aligned} \quad (5)$$

which is required, in the shell model, to account for the nonlinear terms in (4). Eq. (5) is the generalization to two arguments of the nonlinear coupling (giving rise to the energy flux in spectral space) of the so called ‘‘Sabra model’’ [70]. In terms of (5), the shell model for the Eqs. (4) can be written as:

$$\begin{aligned} \dot{u}_n &= \frac{i}{3} \Phi_n^{(\varepsilon)}(u, u) - \gamma_u(k_n)u_n + f_n^{(a)} \\ \dot{p}_n &= \frac{i}{3} \Phi_n^{(\varepsilon)}(u, p) + \frac{i}{3} w \Phi_n^{(\varepsilon)}(p, p) - \frac{i}{3} \Phi_n^{(\varepsilon)}(p, u) \\ &\quad - \gamma_p(k_n)p_n - \Gamma p_n. \end{aligned} \quad (6)$$

The set of wavenumbers is taken to be $k_n = k_0 2^n$. The linear damping terms stem from dissipation ($\gamma_u(k_n)u_n$) and diffusion ($\gamma_p(k_n)p_n$), and the coefficients read $\gamma_u(k_n) = \nu_{u,p}k_n^2 + \mu_{u,p}k_n^{-4}$, where $\nu_{u,p}$ are the actual viscosity and diffusion coefficient, acting at small scales (large wavenumbers), whereas $\mu_{u,p}$ are large scale drag coefficients, mimicking friction with the boundaries [60, 71]. The parameter ε determines the sign of the flux of generalized ‘‘energy’’ across shells, i.e. whether the kinetic energy, $|u_n|^2$, or, alternatively, the orientation magnitude, $|p_n|^2$, are transferred from large to small scales (as it is, for instance, in actual inertial, three-dimensional, turbulence) or vice versa. In particular, for $\varepsilon_c < \varepsilon < 0$ downwards transfer is supported (the so called *direct cascade*), whereas for $\varepsilon < \varepsilon_c = -1 - 2^{-2/3}$ [71] upwards transfer (the *inverse cascade*) takes place. Deciding which is the direction of transfer of fluctuations is not an obvious task; an analog of the Richardson picture [19], that implies a direct cascade in 3d inertial turbulence, is, in fact, missing for active turbulence. We need, then, to propose an equivalent phenomenology that goes as follows. First of all, let us notice that, owing to the typically viscous character of collective phenomena in active fluids, no transfer whatsoever can be ascribed to the non-linear term in the shell model version of the Navier-Stokes equation. To enforce the zero Reynolds number condition, therefore, we set $\Phi_n^{(\varepsilon)}(u, u) = 0 \quad \forall n$ in (6). The velocity dynamics in active turbulence is, actually, governed by a scale-matched balance of active forcing and viscous dissipation [22, 24]; therefore, to the divergence of the active stress $\sigma^{(a)}$ in (4), a *local-in-scale* (or, equivalently, in wavenumber) force must correspond in the shell model, whence $\nabla \cdot \sigma^{(a)} \rightarrow f_n^{(a)} = ik_n \zeta p_n^2$. A different mechanism, promoting the emergence of collective motion in the system and hence involving the P -equation, should, then, excite the multiple scales in the fluid, i.e. generates the *turbulence*. Such a mechanism can be identified in the flow alignment, whereby the velocity gradients are coupled to the orientational degrees of freedom of the microswimmers [35, 64, 72]. We conjecture, then, that the *rotation* term, $p \nabla u$, is the one responsible for the upwards transfer and we set $\varepsilon = \varepsilon_b < \varepsilon_c$ in the operator $\Phi_n^{(\varepsilon)}(p, u)$ in (6). On the other hand, we expect that the advective, $u \nabla p$, and self-advective, $p \nabla p$, terms have mixing properties that should tend to disrupt spatial coherence of orientation and, therefore, to transfer downwards. We want to justify empirically these assumptions *a posteriori*, benchmarking them against direct numerical simulations. Since our numerical method couples a Lagrangian dynamics for microswimmers with a Eulerian description of the fluid, though, first we need a procedure that maps the particle positions and

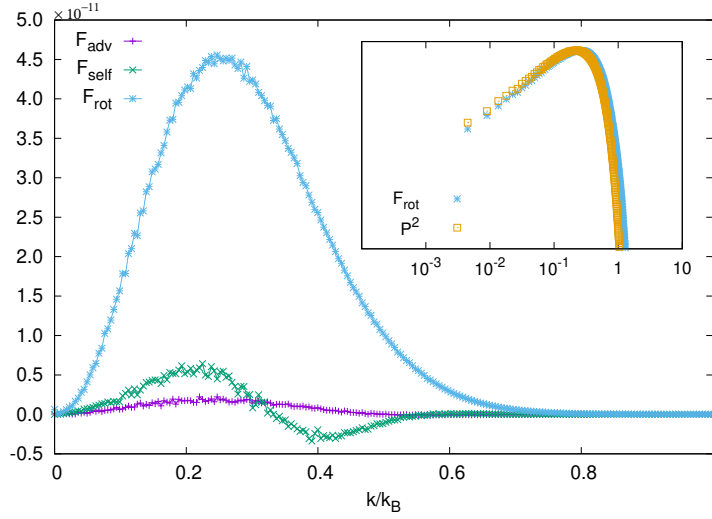


FIG. 3. Spectral fluxes, Eq. (9), measured from the numerical simulations (time-averaged over the statistically stationary state). In the inset we check the expected proportionality between \mathcal{F}_{rot} and \mathcal{P} , thus validating Eq. (12) in the direct numerical simulations (\mathcal{P} is scaled by a factor $\sim 2.6 \times 10^{-4}$).

orientations to the field \mathbf{P} . The latter is reconstructed with the aid of a Gaussian kernel according to the expression:

$$\mathbf{p}(\mathbf{x}, t) = \sum_{i=1}^N G(|\mathbf{x} - \mathbf{X}_i(t)|) \hat{\mathbf{e}}_i, \quad (7)$$

where $G(\xi) = Ae^{-(\xi/R)^2}$ and A is a prefactor such that $\int G(\xi) d^3\xi = 1$. At this point, by projecting the second of Eqs. (4) onto the Fourier mode \mathbf{k} , multiplying both sides by $\tilde{\mathbf{p}}^*$ (the complex conjugate of the Fourier transform of \mathbf{p}), averaging over shells of radius k and summing with the complex conjugate equation, we get:

$$(\partial_t + \Gamma + Dk^2)\mathcal{P} = \mathcal{F}_{\text{adv}} + \mathcal{F}_{\text{self}} + \mathcal{F}_{\text{rot}}, \quad (8)$$

where $\mathcal{P}(k, t) = \langle |\tilde{\mathbf{p}}|^2 \rangle$. The terms on the right hand side read as follows:

$$\begin{aligned} \mathcal{F}_{\text{adv}}(k, t) &= -\langle (\tilde{\mathbf{p}}^*(\mathbf{k}, t) \cdot \mathbf{J}_{\text{up}}(\mathbf{k}, t)) \rangle + \text{c.c.} \\ \mathcal{F}_{\text{self}}(k, t) &= -\langle (\tilde{\mathbf{p}}^*(\mathbf{k}, t) \cdot \mathbf{J}_{\text{pp}}(\mathbf{k}, t)) \rangle + \text{c.c.} \\ \mathcal{F}_{\text{rot}}(k, t) &= \langle (\tilde{\mathbf{p}}^*(\mathbf{k}, t) \cdot \mathcal{R}(\mathbf{k}, t)) \rangle + \text{c.c.} \end{aligned} \quad (9)$$

where $\mathbf{J}_{\text{up}}(\mathbf{k}, t)$, $\mathbf{J}_{\text{pp}}(\mathbf{k}, t)$ and $\mathcal{R}(\mathbf{k}, t)$ are the Fourier transforms of the non-linear terms of the orientation field equation, namely $\mathbf{u} \cdot \nabla \mathbf{p}$, $w \mathbf{p} \cdot \mathbf{p}$ and $\boldsymbol{\Omega} \cdot \mathbf{p}$, respectively, and "c.c." stands for the complex conjugate terms. Eqs. (9) are fluxes across k -shells in spectral space and whether a direct or inverse *cascade of magnitude of orientation*, depending on their sign, takes place. We measured them in the numerical simulations and the results, averaged in time over the statistically stationary state are plotted in Fig. 3. We see that, while \mathcal{F}_{adv} and $\mathcal{F}_{\text{self}}$ (top and middle panels) are negative at intermediate and large wavenumbers, signalling that they transfer orientation fluctuations towards small scales (i.e. they tend to disrupt coherence), the rotational spectral flux \mathcal{F}_{rot} (bottom panel) is positive (and in magnitude much larger than the previous two), therefore confirming our phenomenological conjecture that it is the term responsible for the upward *cascade* that eventually pumps energy into the large scales. We set, then, $\varepsilon = \varepsilon_f > \varepsilon_c$ in the operators $\Phi_n^{(\varepsilon)}(u, p)$ and $\Phi_n^{(\varepsilon)}(p, p)$ in (6). Eventually, we arrive at the following structure for the sought *SabrActive* shell model:

$$\begin{aligned} \dot{u}_n &= -\gamma_u(k_n)u_n + i\zeta k_n p_n^2 \\ \dot{p}_n &= \frac{i}{3}\Phi_n^{(\varepsilon_f)}(u, p) + \frac{i}{3}w\Phi_n^{(\varepsilon_f)}(p, p) - \frac{i}{3}\Phi_n^{(\varepsilon_b)}(p, u) \\ &\quad - \gamma_p(k_n)p_n - \Gamma p_n + \delta_{n, n_B}|p_n|^{-1}p_n p_B. \end{aligned} \quad (10)$$

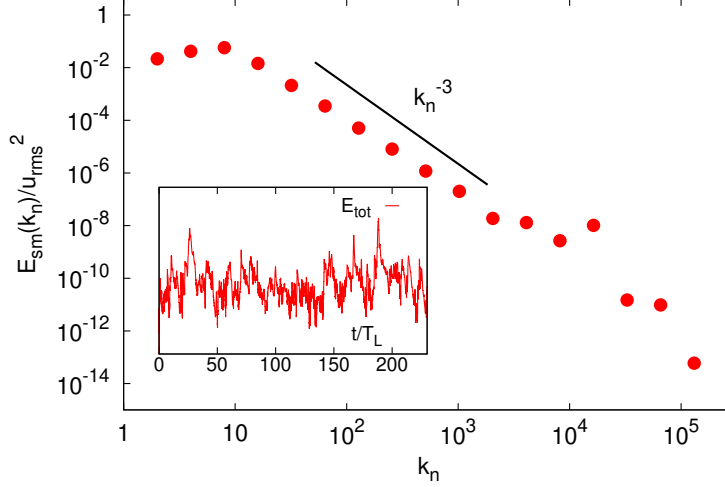


FIG. 4. MAIN PANEL: Time-averaged (over the steady state) energy spectrum, normalized by the mean square velocity $u_{\text{rms}}^2 = \sum_n |u_n|^2$, from the simulation of the shell model for active turbulence, Eq. (10). INSET: Total energy, $E_{\text{tot}}(t) = \sum_n |u_n|^2$, vs time (in units of the integral scale characteristic time $T_L = (k_{\text{max}} u_{\text{rms}})^{-1}$).

The *forcing* term $\delta_{n,n_B} |p_n|^{-1} p_n p_B$ has been introduced in the p -equation to account for the fact that at the smallest scale (ideally that of a bacterium) the orientation is fixed by the intrinsic microorganism swimming direction.

We integrated the system (10) with $N_s = 20$ shells by means of a fourth-order Runge-Kutta scheme for $T = 6 \times 10^{11}$ time steps (with integration step $\Delta t = 10^{-4}$), corresponding to $\approx 200 T_L$, $T_L = (k_{\text{max}} u_{\text{rms}})^{-1}$ being the large scale characteristic time, where $u_{\text{rms}} = (\sum_n |u_n|^2)^{1/2}$ and k_{max} is the location of spectrum maximum (i.e. the wavenumber of the energy-containing scales) [73]. The following numerical values are used for the parameters: $k_0 = 2^{-4}$, $\varepsilon_f = -0.4$, $\varepsilon_b = -1.8$, $\nu_u = 10^{-6}$, $\mu_u = 10^{-10}$, $\zeta = 1.25 \times 10^{-2}$, $w = 1.25 \times 10^{-2}$, $\nu_p = 8.5 \times 10^{-13}$, $\mu_p = 10^{-10}$, $\Gamma = 10^{-6}$, $p_B = 5 \times 10^{-11}(1+i)$, $n_B = N_s - 1$.

Fig. 4 displays the energy spectrum, $E_{\text{sm}}(k_n) = \langle \frac{|u_n|^2}{k_n} \rangle$, for the shell model, where the average, $\langle \dots \rangle$ is meant taken over time, in the statistically stationary state $t \gtrsim 10 T_L$ (see inset of Fig. 4 displaying the total energy, $E_{\text{tot}}(t) = \sum_n |u_n|^2$, as a function of time). The spectrum decays over a quite wide range of wavenumbers as $E_{\text{sm}}(k_n) \sim k_n^{-3}$ (solid line in Fig. 4), in agreement with the DNS. Moreover, the shell model allows to provide a theoretical explanation of such power law decay. To this aim, let us obtain the evolution of the orientation magnitude, $|p_n|^2$, by multiplying the second of Eqs. (10) by p_n^* and its complex conjugate by p_n and summing the two:

$$\partial_t |p_n|^2 \approx p_n^* \Phi_n^{(\varepsilon_b)}(p, u) + p_n (\Phi_n^{(\varepsilon_b)}(p, u))^* - \Gamma |p_n|^2 - \gamma(k_n) |p_n|^2. \quad (11)$$

Here the advective and self-advecting terms have been omitted, since they are much smaller than the rotation, as observed in the (see Fig. 3). Assuming statistical stationarity and focusing on intermediate k_n , where diffusive terms can be neglected, we see that

$$k u p^2 \sim \Gamma p^2. \quad (12)$$

From Eq. (12) we get $u \sim k^{-1}$ and, then, the energy spectrum, $k_n^{-1} |u_n|^2$, should indeed behave as

$$E_{\text{sm}}(k_n) \sim k_n^{-3}. \quad (13)$$

IV. CONCLUSIONS

We have presented a computational and theoretical study aimed at revealing the presence of active turbulence in pusher suspensions in conditions of semi-dilution, namely far from close packing but above the onset of collective motion. We reported that the Eulerian solvent velocity is Lévy-distributed, similarly to previous experimental and theoretical results [54, 55]. We showed that the energy spectrum develops decays with the power-law k^{-3} over a

range of intermediate wavenumbers. It was posited that, given the lack of a Richardson-Kolmogorov energy cascade as in classical turbulence, the excitation of motion at large scales should be ascribed to the coupling between fluid velocity gradients and microswimmer orientation, i.e. to the flow alignment mechanism. Based on this picture and on phenomenological arguments, we developed a reduce order dynamical deterministic model (or *shell model*) of active turbulence, dubbed *SabrActive model*. Numerical simulations and theoretical analysis of the model confirmed the k^{-3} scaling of the spectrum.

The introduction of this new model pushes forward the reach of quantitative tests of how actually "turbulent" is active turbulence, allowing to measure, e.g., Lyapunov exponents, higher order structure functions, multiscale statistics, etc, on "physically" much longer runs. A flavour of this capability can be grasped in the observation of intermittency in the PDFs of shell model velocity variables. The insight provided will motivate further analysis of the dynamical and statistical properties of the model and the sensitivity of the system response to changes in the control parameters (for instance, the onset of active turbulence at changing the "activity parameter"), as well as exploring a wider region of the volume-fraction/squirming-parameters space in DNS.

ACKNOWLEDGEMENTS

I.P. acknowledges support from Ministerio de Ciencia, Innovación y Universidades MCIU/AEI/FEDER for financial support under grant agreement PID2021-126570NB-I00 AEI/FEDER-EU, from Generalitat de Catalunya under Program Icrea Acadèmia and project 2021SGR-673. This work was possible thanks to the access to the MareNostrum Supercomputer at Barcelona Supercomputing Center (BSC) and also through the Partnership for Advanced Computing in Europe (PRACE).

-
- [1] T Vicsek and A. Zafeiris, "Collective motion," *Phys. Rep.* **517**, 71–149 (2012).
 - [2] D.B. Kearns, "A field guide to bacterial swarming motility," *Nat. Rev. Microbiol.* **8**, 634–644 (2010).
 - [3] N.C. Darnton, L. Turner, S. Rojevsky, and H.C. Berg, "Dynamics of bacterial swarming," *Biophys. J.* **98**, 2082–2090 (2010).
 - [4] D.L. Koch and G. Subramanian, "Collective hydrodynamics of swimming microorganisms: living fluids," *Annu. Rev. Fluid Mech.* **43**, 637–659 (2011).
 - [5] M. Ballerini, N. Cabibbo, R. Candelier, A. Cavagna, E. Cisbani, I. Giardina, V. Lecomte, A. Orlandi, G. Parisi, A. Procaccini, M. Viale, and V. Zdravkovic, "Interaction ruling animal collective behavior depends on topological rather than metric distance: Evidence from a field study," *Proc. Natl. Acad. Sci. USA* **105**, 1232–1237 (2008).
 - [6] J.E. Herbert-Read, A. Perna, R.P. Mann, T.M. Schaerf, D.J.T. Sumpter, and A.J.W. Ward, "Inferring the rules of interaction of shoaling fish," *Proc. Natl. Acad. Sci. USA* **108**, 18726–18731 (2011).
 - [7] C. Dombrowski, L. Cisneros, S. Chatkaew, R.E. Goldstein, and J.O. Kessler, "Self-concentration and large-scale coherence in bacterial dynamics," *Phys. Rev. Lett.* **93**, 098103 (2004).
 - [8] C.W. Wolgemuth, "Collective swimming and the dynamics of bacterial turbulence," *Biophys. J.* **95**, 1564–1574 (2008).
 - [9] T.J. Pedley and J.O. Kessler, "Hydrodynamic phenomena in suspensions of swimming microorganisms," *Annu. Rev. Fluid Mech.* **23**, 313–358 (1992).
 - [10] R. Alert and J.-F. Casademunt, J. Joanny, "Active turbulence," *Annu. Rev. Condens. Matter Phys.* **13**, 143–170 (2020).
 - [11] G.K. Vallis, *Lecture Notes on "Geostrophys turbulence: the macroturbulence of the atmosphere and ocean"* (1999).
 - [12] T. Ishikawa, N. Yoshida, H. Uedo, M. Wiedemann, Y. Imai, and T. Yamaguchi, "Energy transport in a concentrated suspension of bacteria," *Phys. Rev. Lett.* **107**, 028102 (2011).
 - [13] H.H. Wensink, J. Dunkel, S. Heidenreich, K. Drescher, R.E. Goldstein, H. Löwen, and J.M. Yeomans, "Meso-scale turbulence in living fluids," *Proc. Natl. Acad. Sci. USA* **109**, 14308–14313 (2012).
 - [14] G. Kokot, S. Das, R.G. Winkler, G. Gompper, I.S. Aranson, and A. Snezhko, "Active turbulence in a gas of self-assembled spinners," *Proc. Natl. Acad. Sci. USA* **112**, 15048–15053 (2015).
 - [15] A. Doostmohammadi, T.N. Shendruk, K. Thijssen, and J.M. Yeomans, "Onset of meso-scale turbulence in active nematics," *Nat. Commun.* **8**, 15326 (2017).
 - [16] B. Martínez-Prat, R. Alert, F. Meng, J. Ignés-Mullol, J.-F. Joanny, J. Casademunt, R. Golestanian, and F. Sagués, "Scaling regimes of active turbulence with external dissipation," *Phys. Rev. X* **11**, 031065 (2021).
 - [17] M. Bourgoïn, R. Kervil, C. Cottin-Bizonne, R. Raynal, R. Volk, and C. Ybert, "Kolmogorovian active turbulence of a sparse assembly of interacting marangoni surfers," *Phys. Rev. X* **10**, 021065 (2020).
 - [18] V. Bratanov, F. Jenko, and E. Frey, "New class of turbulence in active fluids," *Proc. Natl. Acad. Sci. USA* **112**, 15048–15053 (2015).
 - [19] U. Frisch, *Turbulence* (Cambridge University Press, 1995).

- [20] L. Ślomka and J. Dunkel, “Spontaneous mirror-symmetry breaking induces inverse energy cascade in 3d active fluids,” *Proc. Natl. Acad. Sci. USA* **114**, 2119–2124 (2017).
- [21] M. Linkmann, G. Boffetta, M.C. Marchetti, and B. Eckhardt, “Phase transition to large scale coherent structures in two-dimensional active matter turbulence,” *Phys. Rev. Lett.* **122**, 214503 (2019).
- [22] L.N. Carenza, L. Biferale, and G. Gonnella, “Multiscale control of active emulsion dynamics,” *Phys. Rev. Fluid* **5**, 011302(R) (2020).
- [23] L.N. Carenza, L. Biferale, and G. Gonnella, “Cascade or not cascade? energy transfer and elastic effects in active nematics,” *Europhys. Lett.* **132**, 44003 (2020).
- [24] R. Alert, J.-F. Joanny, and J. Casademunt, “Universal scaling of active nematic turbulence,” *Nat. Phys.* **16**, 682–688 (2020).
- [25] C. Rorai, F. Toschi, and I. Pagonabarraga, “Coexistence of active and hydrodynamic turbulence in two-dimensional active nematics,” *Phys. Rev. Lett.* **129**, 218001 (2022).
- [26] K. Kruse, J.F. Joanny, F. Jülicher, J. Prost, and K. Sekimoto, “Asters, vortices and rotating spirals in active gels of polar filaments,” *Phys. Rev. Lett.* **92**, 078101 (2004).
- [27] L. Giomi, M.C. Marchetti, and T.B. Liverpool, “Complex spontaneous flows and concentration banding in active polar films,” *Phys. Rev. Lett.* **101**, 198101 (2008).
- [28] S.A. Edwards and J.M. Yeomans, “Spontaneous flow states in active nematics: A unified picture,” *Europhys. Lett.* **85**, 18008 (2008).
- [29] E. Tjhung, M.E. Cates, and D. Marenduzzo, “Nonequilibrium steady states in polar active fluids,” *Soft Matter* **7**, 7453–7464 (2011).
- [30] L. Ślomka and J. Dunkel, “Generalized navier-stokes equations for active suspensions,” *Eur. Phys. J. Spec. Top.* **224**, 1349–1358 (2015).
- [31] J. Stenhammar, C. Nardini, R.W. Nash, D. Marenduzzo, and A. Morozov, “Role of correlations in the collective behavior of microswimmer suspensions,” *Phys. Rev. Lett.* **119**, 028005 (2017).
- [32] D. Bárdfalvy, H. Nordanger, C. Nardini, A. Morozov, and J. Stenhammar, “Particle-resolved lattice boltzmann simulations of 3-dimensional active turbulence,” *Soft Matter* **15**, 7747–7756 (2019).
- [33] V. Škultéty, C. Nardini, J. Stenhammar, D. Marenduzzo, and A. Morozov, “Swimming suppresses correlations in dilute suspensions of pusher microorganisms,” *Phys. Rev. X* **10**, 031059 (2020).
- [34] X.-L. Wu and A. Libchaber, “Particle diffusion in a quasi-two-dimensional bacterial bath,” *Phys. Rev. Lett.* **84**, 3017–3020 (2000).
- [35] J.P. Hernández-Ortiz, C.G. Stoltz, and M.D. Graham, “Transport and collective dynamics in suspensions of confined swimming particles,” *Phys. Rev. Lett.* **95**, 204501 (2005).
- [36] K.C. Leptos, J.S. Guasto, J.P. Gollub, A.I. Pesci, and R.E. Goldstein, “Dynamics of enhanced tracer diffusion in suspensions of swimming eukaryotic microorganisms,” *Phys. Rev. Lett.* **103**, 198103 (2009).
- [37] D. Saintillan and M.J. Shelley, “Emergence of coherent structures and large-scale flows in motile suspensions,” *J. R. Soc. Interface* **9**, 571–585 (2012).
- [38] L. Biferale, “Shell models of energy cascade in turbulence,” *Annu. Rev. Fluid Mech.* **35**, 441–468 (2004).
- [39] S. Succi, *The lattice Boltzmann equation for complex state of flowing matter* (Oxford University Press, 2018).
- [40] D.A. Wolf-Gladow, *Lattice-gas cellular automata and lattice Boltzmann models. An introduction* (Springer, 2000).
- [41] J.-C. Desplat, I. Pagonabarraga, and P. Bladon, “Ludwig: A parallel lattice-boltzmann code for complex fluids,” *Comp. Phys. Commun.* **134**, 273–290 (2001).
- [42] A.J.C. Ladd, “Numerical simulations of particulate suspensions via a discretized boltzmann equation. part 1. theoretical foundation,” *J. Fluid Mech.* **271**, 285–309 (1994).
- [43] N.Q. Nguyen and A.J.C. Ladd, “Lubrication corrections for lattice-boltzmann simulations of particle suspensions,” *Phys. Rev. E* **66**, 046708 (2002).
- [44] C.K. Aidun and J.R. Clausen, “Lattice-boltzmann method for complex flows,” *Annu. Rev. Fluid Mech.* **42**, 439–472 (2010).
- [45] J.R. Blake, “A spherical envelope approach to ciliary propulsion,” *J. Fluid Mech.* **46**, 199–208 (1971).
- [46] T. Ishikawa, M.P. Simmonds, and T.J. Pedley, *J. Fluid Mech.* **568**, 119–160 (2006).
- [47] R. Matas Navarro and I. Pagonabarraga, *Eur. Phys. J. E* **33**, 27–39 (2010).
- [48] F. Alarcón and I. Pagonabarraga, “Spontaneous aggregation and global polar ordering in squirmer suspensions,” *J. Mol. Liq.* **185**, 56–61 (2013).
- [49] F. Alarcón, C. Valeriani, and I. Pagonabarraga, “Morphology of clusters of attractive dry and wet self-propelled spherical particle suspensions,” *Soft Matter* **13**, 814–826 (2017).
- [50] A. Scagliarini and I. Pagonabarraga, “Hydrodynamic and geometric effects in the sedimentation of model run-and-tumble microswimmers,” *Soft Matter* **18**, 2407–2413 (2022).
- [51] A.A. Evans, T. Ishikawa, T. Yamaguchi, and E. Lauga, “Orientational order in concentrated suspensions of spherical microswimmers,” *Phys. Fluids* **23**, 111702 (2011).
- [52] Z. Liu, W. Zeng, X. Ma, and X. Cheng, “Density fluctuations and energy spectra of 3d bacterial suspensions,” *Soft Matter* **17**, 10806–10817 (2021).
- [53] S.-Z. Lin, W.-Y. Zhang, D. Bi, B. Li, and X.-Q. Feng, “Energetics of mesoscale cell turbulence in two-dimensional monolayers,” *Commun. Phys.* **4**, 21 (2021).
- [54] I.M. Zaid, J. Dunkel, and J.M. Yeomans, “Lévy fluctuations and mixing in dilute suspensions of algae and bacteria,” *J. R. Soc. Interface* **8**, 1314–1331 (2011).

- [55] I. Rushkin, V. Kantsler, and R.E. Goldstein, “Fluid velocity fluctuations in a suspension of swimming protists,” *Phys. Rev. Lett.* **105**, 188101 (2010).
- [56] E.B. Gledzer, “System of hydrodynamic type admitting two quadratic integrals of motion,” *Sov. Phys. Dokl.* **18**, 216–217 (1973).
- [57] V.N. Desnyansky and E.A. Novikov, “The evolution of turbulence spectra to the similarity regime,” *Izv. Akad. Nauk SSSR Fiz. Atmos. Okeana* **10**, 127–136 (1974).
- [58] T. Bohr, M.H. Jensen, G. Paladin, and A. Vulpiani, *Dynamical systems approach to turbulence* (Cambridge University Press, 1998).
- [59] R. Benzi, E. De Angelis, R. Govindarajan, and I. Procaccia, “Shell model of drag reduction with polymer additives in homogeneous turbulence,” *Phys. Rev. E* **68**, 016308 (2003).
- [60] R. Benzi, N. Horesh, and I. Procaccia, “Shell model of two-dimensional turbulence in polymer solutions,” *Europhys. Lett.* **68**, 310–315 (2004).
- [61] S.S. Ray and D. Vincenzi, “Elastic turbulence in a shell model of polymer solution,” *Europhys. Lett.* **144**, 44001 (2016).
- [62] The system for the velocity variables is coupled, in this case, to a set of equations for analogous *polymer* variables, interpreted as spectral amplitudes of an auxiliary vector field whose dyadic product is the polymer conformation tensor [59].
- [63] N. Yoshinaga and T.B. Liverpool, “Hydrodynamic interactions in dense active suspensions: From polar order to dynamical clusters,” *Phys. Rev. E* **96**, 020603(R) (2017).
- [64] R. Aditi Simha and S. Ramaswamy, “Hydrodynamic fluctuations and instabilities in ordered suspensions of self-propelled particles,” *Phys. Rev. Lett.* **89**, 058101 (2002).
- [65] Y. Hatwalne, S. Ramaswamy, M. Rao, and R. Aditi Simha, “Rheology of active-particle suspensions,” *Phys. Rev. Lett.* **92**, 118101 (2004).
- [66] D. Saintillan and M.J. Shelley, “Instabilities and pattern formation in active particle suspensions: kinetic theory and continuum simulations,” *Phys. Rev. Lett.* **100**, 178103 (2008).
- [67] D. Saintillan and M.J. Shelley, “Instabilities, pattern formation, and mixing in active suspensions,” *Phys. Fluids* **20**, 123304 (2008).
- [68] A. Baskaran and M.C. Marchetti, “Statistical mechanics and hydrodynamics of bacterial suspensions,” *Proc. Natl. Acad. Sci. USA* **106**, 15567–15572 (2009).
- [69] R.B. Bird, R.C. Armstrong, and O. Hassager, *Dynamics of Polymeric Liquids* (John Wiley and sons, 1987).
- [70] V.S. L’vov, E. Podivilov, A. Pomyalov, I. Procaccia, and D. Vandembroucq, “Improved shell model of turbulence,” *Phys. Rev. E* **58**, 1811–1822 (1998).
- [71] T. Gilbert, V.S. L’vov, A. Pomyalov, and I. Procaccia, “Inverse cascade regime in shell models of two-dimensional turbulence,” *Phys. Rev. Lett.* **89**, 074501 (2002).
- [72] D. Saintillan and M.J. Shelley, “Orientational order and instabilities in suspensions of self-locomoting rods,” *Phys. Rev. Lett.* **99**, 058102 (2007).
- [73] D. Pisarenko, L. Biferale, D. Courvoisier, U. Frisch, and M. Vergassola, “Further results on multifractality in shell models,” *Phys. Fluids* **5**, 2533–2538 (1993).